Longitudinal collective modes in asymmetric charged-particle bilayers

2006 J. Phys. A: Math. Gen. 39 4601

(http://iopscience.iop.org/0305-4470/39/17/S45)

INSTITUTE OF PHYSICS PUBLISHING JOURNAL OF PHYSICS A: MATHEMATICAL AND GENERAL

J. Phys. A: Math. Gen. **39** (2006) 4601–4605 doi:10.1088/0305-4470/39/17/S45

Longitudinal collective modes in asymmetric charged-particle bilayers

Hania Mahassen[1], **Kinga Kutasi**[2], **Kenneth I Golden**[1], **Gabor J Kalman**[3] and **Zoltan Donko**[2]

[1] Department of Mathematics and Statistics, University of Vermont, Burlington, VT 05401-1455 USA

[2] Research Institute for Solid State Physics and Optics, Hungarian Academy of Sciences, H-1525 Budapest, PO Box 49, Hungary

[3] Department of Physics, Boston College, Chestnut Hill, MA 02467 USA

E-mail: golden@emba.uvm.edu

Received 22 August 2005, in final form 22 December 2005
Published 7 April 2006
Online at stacks.iop.org/JPhysA/39/4601

Abstract

We have analysed the dispersion of longitudinal collective modes in classical asymmetric charged-particle bilayer liquids in the strong coupling regime. The theoretical analysis is based on a dielectric matrix calculated in the quasi-localized charge approximation (QLCA). The matrix elements are expressed as integrals over inter-layer and intra-layer pair correlation function data that we have generated by molecular dynamics (MD) simulations. At the same time, MD simulations of density and current fluctuation spectra were analysed to infer the collective mode dispersion. The long-wavelength finite frequency (energy) gap, brought about by strong inter-layer correlations, is a monotonically increasing function of the density ratio, n_2/n_1, and, for the smallest value of the inter-layer spacing considered, the gap reaches its maximum value when the two layer densities are equal. It appears that it stays at that value for $n_2/n_1 > 1$.

PACS numbers: 52.27.Gr, 52.25.Mq, 52.35.Fp

1. Introduction

Studies of the dynamic properties of strongly coupled charged-particle bilayers have, for the most part, been confined to symmetric ($n_1 = n_2$) bilayers. Addressing the collective mode behaviour, which is of interest in the present work, the symmetric bilayer features four modes: two (longitudinal and transverse) in-phase (+) modes and two (longitudinal and transverse) out-of-phase (−) modes. For weak coupling, the random-phase approximation (RPA) predicts that the (−) mode exhibits an acoustic ($\omega \propto k$) behaviour for $k \to 0$. In contrast, for strong

Table 1. QLCA and MD values of the $k \to 0$ finite-frequency energy gap as a function of the n_2/n_1 density ratios; $\Gamma_1 = 50, d/a_1 = 0.3$; $\omega_{\mathrm{GAP}}^{\mathrm{sym}} = \sqrt{2\pi ne^2 l/m}$ is the gap frequency of the symmetric bilayer. $\omega_0^2 = \pi e^2/m(n_1/a_1 + n_2/a_2)$; $\pi a_i^2 n_i^2 = 1$.

n_2/n_1	QLCA $\omega_{\mathrm{GAP}}/\omega_0$	MD $\omega_{\mathrm{GAP}}/\omega_0$	QLCA $\omega_{\mathrm{GAP}}/\omega_{\mathrm{GAP}}^{\mathrm{sym}}$	MD $\omega_{\mathrm{GAP}}/\omega_{\mathrm{GAP}}^{\mathrm{sym}}$
1/16	0.943	1.207	0.611	0.637
5/16	0.989	1.331	0.728	0.755
1	1.040	1.350	1.000	1.000
24/16	1.018	1.343	1.165	1.185

coupling, our own theoretical and molecular dynamics (MD) studies [1–4], as well as the MD simulations carried out by Ranganathan and Johnson [5], show that for $k \to 0$, a finite-frequency gap develops.

The question arises: how is the collective mode dispersion modified when $n_1 \neq n_2$? The asymmetry question was addressed some time ago by Vitlina and Chaplick [6, 7] and, more recently, by Kulik *et al* [8] in the context of an RPA description of the electron bilayer in the zero-temperature quantum domain. By contrast, the present work addresses this question in the context of a QLCA (quasi-localized-charge approximation) description [1, 2, 9] of the strongly coupled charged-particle bilayer in the classical domain. The most important issue here is the variation of the energy gap with density ratio n_2/n_1 as described in table 1 and figure 3. As to the topology of the (+) and (−) dispersion curves, we will see that, in contrast to the symmetric bilayer, the present theory predicts that the two dispersion curves can never intersect nor can the corresponding eigenvectors have fixed in-phase and out-of-phase polarizations. This latter behaviour is by no means unique to the QLCA [6] and is the result of the breaking of the equal-density symmetry.

2. QLCA dielectric matrix

We consider a charged-particle bilayer described by a model that consists of two unequal-density charged-particle layers of zero thickness, spaced at a distance d apart. Each 2D layer contains a classical Coulomb liquid neutralized by its own rigid uniform positive background. The elements of the interaction matrix are $\phi_{11}(k) = \phi_{22}(k) = 2\pi e^2/k$, $\phi_{12}(k) = [2\pi e^2/k]\exp(-kd)$. $\Gamma_i = \beta e^2/a_i$ is taken to be the customary measure of the coupling strength in layer i; $1/\beta$ is the temperature in energy units and $a_i = 1/\sqrt{\pi n_i}$.

The derivation of the dielectric matrix $\epsilon_{ij}(\mathbf{k}, \omega)$ proceeds from the QLCA equation of motion relating the induced average charge density response ρ_i in layer i to the external charge density perturbation ρ_l^{ext} in layer l.

$$\rho_i(\mathbf{k}, \omega) = [\omega^2 \mathbf{I} - \mathbf{C}(\mathbf{k})]^{-1}_{i\bar{j}} \frac{n_{\bar{j}} k^2}{m} \phi_{\bar{j}\bar{l}}(k) \rho_{\bar{l}}^{\mathrm{ext}}(\mathbf{k}, \omega) \qquad (i, j, l = 1, 2). \tag{1}$$

$\mathbf{I}$ is the (2×2) identity matrix and $\mathbf{C}(\mathbf{k})$ is the dynamical matrix defined by

$$C_{ij}(\mathbf{k}) = \omega_{p_i}\omega_{p_j}\,\mathrm{e}^{-kd(1-\delta_{ij})} + D_{ij}(\mathbf{k}) \qquad (i, j = 1, 2); \tag{2}$$

barred indices denote summation. One obtains the elements of the dielectric matrix

$$\begin{aligned} \epsilon_{11}(\mathbf{k}, \omega) &= 1 - \frac{1}{\Delta(\mathbf{k}, \omega)} \left\{ \omega_{p_1}^2 [\omega^2 - D_{22}(\mathbf{k})] + \omega_{p_1}\omega_{p_2} D_{12}(\mathbf{k})\,\mathrm{e}^{-kd} \right\}, \\ \epsilon_{22} &= \epsilon_{11}(1 \leftrightarrow 2), \end{aligned} \tag{3}$$

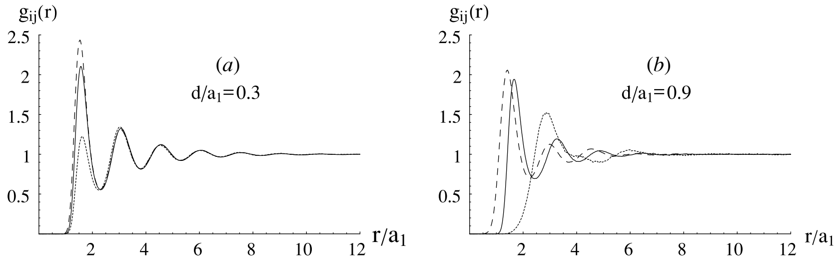

Figure 1. MD pair distribution functions $g_{11}(r)$ (solid curve), $g_{12}(r)$ (dashed curve) and $g_{22}(r)$ (dotted curve); $\Gamma_1 = 50$, $\Gamma_2 = 27.95$, $N_1 = 1600$, $N_2 = 500$.

$$\epsilon_{12}(\mathbf{k},\omega) = -\frac{1}{\Delta(\mathbf{k},\omega)}\left\{\omega_{p_1}\omega_{p_2}D_{12}(\mathbf{k}) + \omega_{p_2}^2[\omega^2 - D_{11}(\mathbf{k})]\,\mathrm{e}^{-kd}\right\}, \qquad \epsilon_{21} = \epsilon_{12}(1 \leftrightarrow 2), \tag{4}$$

where $\Delta(\mathbf{k},\omega) = [\omega^2 - D_{11}(\mathbf{k})][\omega^2 - D_{22}(\mathbf{k})] - [D_{12}(\mathbf{k})]^2$ and $\omega_{p_i} = \sqrt{2\pi n_i e^2 k/m}$ is the 2D plasma frequency in layer i. The $D_{ij}(\mathbf{k})$ account for the inter- and intra-layer Coulomb correlations beyond the RPA

$$D_{11}(\mathbf{k}) = \frac{\pi e^2 n_2}{m}H + \frac{\pi e^2 n_1}{m}\int_0^\infty \mathrm{d}r\,\frac{1}{r^2}h_{11}(r)\left\{1 - 4J_0(kr) + 6\frac{J_1(kr)}{kr}\right\},$$
$$D_{22} = D_{11}(1 \leftrightarrow 2) \tag{5}$$

$$D_{12}(\mathbf{k}) = -\frac{\pi e^2\sqrt{n_1 n_2}}{m}H + \frac{\pi e^2\sqrt{n_1 n_2}}{m}\int_0^\infty \mathrm{d}r\,r h_{12}(r)\frac{1}{(r^2+d^2)^{3/2}}\left\{1 - 4J_0(kr) + 6\frac{J_1(kr)}{kr}\right\}$$
$$- \frac{3\pi e^2\sqrt{n_1 n_2}}{m}\int_0^\infty \mathrm{d}r\,r h_{12}(r)\frac{d^2}{(r^2+d^2)^{5/2}}\left\{1 - 2J_0(kr) + 2\frac{J_1(kr)}{kr}\right\},$$
$$D_{21}(\mathbf{k}) = D_{12}(\mathbf{k}) \tag{6}$$

$$H \equiv H(d) = \int_0^\infty \mathrm{d}r\,r h_{12}(r)\frac{1}{(r^2+d^2)^{3/2}}\left\{1 - \frac{3d^2}{r^2+d^2}\right\}; \tag{7}$$

$h_{ij}(r) = g_{ij}(r) - 1 = (1/N)\sum_k [S_{ij}(\mathbf{k}) - \delta_{ij}]\exp(\mathrm{i}\mathbf{k}\cdot\mathbf{r})$. The $g_{ij}(r)$ are the MD-generated pair distribution functions shown in figure 1. The behaviour of $g_{12}(r)$ relative to $g_{11}(r)$ is qualitatively similar to that found for the symmetric bilayer [10]. The similarity of $g_{11}(r)$ and $g_{22}(r)$ in figure 1(*a*), which is rather surprising in view of the difference between a_1 and a_2, reflects the fact that, for d/a_1 sufficiently small, particles in layer 2 appear in clusters with an inter-particle distance $\approx a_1$. In contrast, for $d/a_1 = 0.9$ (figure 1(*b*)), the layer 2 and layer 1 structures are more independent and the positions of the $g_{22}(r)$ and $g_{11}(r)$ peaks conform to the expected ratio of $\sqrt{N_1/N_2}$.

3. Plasmon dispersion

Turning now to the calculation of the dispersion of the longitudinal excitations, the $\pm$ oscillation frequencies are obtained by setting $\mathrm{Det}[\epsilon(\mathbf{k},\omega)]$ equal to zero:

$$\omega_\pm^2(\mathbf{k}) = \tfrac{1}{2}[C_{11}(\mathbf{k}) + C_{22}(\mathbf{k})] \mp \tfrac{1}{2}\sqrt{[C_{11}(\mathbf{k}) - C_{22}(\mathbf{k})]^2 + 4[C_{12}(\mathbf{k})]^2} \tag{8}$$

Both in the primitive RPA (i.e., RPA where thermal dispersion effects are ignored) that results from equation (8) with the $D_{ij}(\mathbf{k})$ set equal to zero and in the QLCA, the (+) mode exhibits the

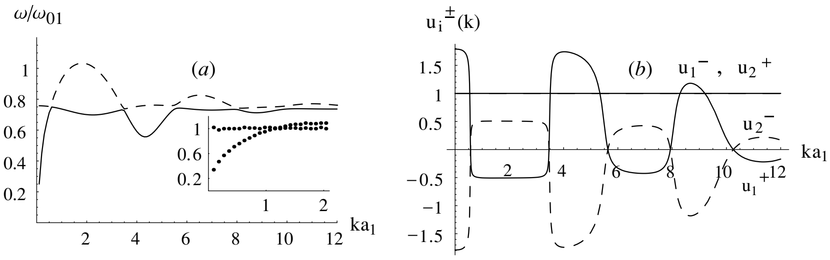

Figure 2. (a) ± QLCA dispersion curves for $\Gamma_1 = 50, \Gamma_2 = 27.95, d/a_1 = 0.3, N_1 = 1600, N_2 = 500$; $\omega_{01} = \sqrt{2\pi n_1 e^2/ma_1}$. The (+) and (−) modes are represented by the solid and dashed curves, respectively. The inset shows MD dispersion data ω/ω_{01} as a function of ka_1; the apparent intersection of the two modes is probably spurious and is due to the lack of sufficient resolution. (b) $\mathbf{u}^{\pm}$ eigenvectors as functions of ka_1 calculated from equation (1); $\mathbf{u}^{+}(k) = [u_1^{+}(k), 1], \mathbf{u}^{-}(k) = [1, u_2^{-}(k)]$.

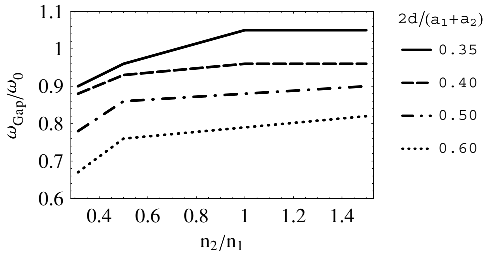

Figure 3. QLCA energy gap frequency as a function of density ratio n_2/n_1 for different inter-layer separations: $\omega_0^2 = \pi e^2/m(n_1/a_1 + n_2/a_2)$; $\pi a_i^2 n_i^2 = 1$.

well-known $\omega_+ \propto \sqrt{k}$ dispersion in the $k \to 0$ limit. However, the primitive RPA and QLCA descriptions of the (−) mode in this limit differ dramatically: in the RPA description, $\omega_-(k \to 0) \propto k$, whereas in the QLCA description, $\omega_-(k \to 0) \equiv \omega_{\mathrm{GAP}} = \sqrt{(\pi e^2/m)(n_1 + n_2)H}$.

There is one notable difference in the QLCA description of plasmon dispersion in symmetric and asymmetric bilayers. In the symmetric case, the (+) and (−) curves intersect to form a braided structure [1, 2] with the dispersion terminating in a single Einstein frequency at large k. In this case, one can define the (+) and (−) modes by requiring continuous derivatives across the intersections; with this definition, the (+) mode is always in-phase and the (−) mode is always out-of-phase. In the asymmetric case, the (+) and (−) dispersion curves also assume the braided structure, but can never quite intersect (see figure 2(a)), and they terminate in two distinct Einstein frequencies. Similarly to what occurs in the RPA [6, 7], the corresponding (+) and (−) eigenvectors are k-dependent (see figure 2(b)), i.e. they do not have fixed in-phase and out-of-phase polarizations. We note that the abrupt changes in the polarizations occur near the points of closest contact between the ± dispersion curves.

The MD dispersion data (inset to figure 2(a)) for $ka_1 \lesssim 0.6$ are in good correspondence with the (+) theory curve and for $0.7 \lesssim ka_1 \lesssim 1.4$ with the (−) theory curve. Both theory and MD data show an energy gap. However, the QLCA theory predicts an energy gap that is approximately 25–30% lower than the MD value. We do not yet understand the origin of this discrepancy which has also been reported in the symmetric bilayer [3]. Nonetheless, table 1 shows that, over the studied range of density ratios, there is consistently a good agreement between the QLCA and MD gap-frequency ratios $\omega_{\mathrm{GAP}}/\omega_{\mathrm{GAP}}^{\mathrm{sym}}$. We see from figure 3 that, not surprisingly, the energy gap increases with increasing density ratio for a fixed inter-layer spacing. For the smallest value of 0.35, the dimensionless gap frequency ultimately reaches a maximum value of 1.05 and appears to stay at that value thereafter.

The variation of the energy gap with density ratio, the marked contrast between the topologies of the QLCA and RPA [6, 7] dispersion curves, and the MD generated $g_{ij}(r)$ data (figure 1) and dispersion curves (figure, 2 inset) are the principal new results of the present paper.

Acknowledgments

This work has been supported by grants NSF PHY-0206554, NSF PHY-0514618, NSF PHY-0206695, NSF PHY-0514619, OKTA-T-48389 and MTA-OTKA-90/46140.

References

[1] Kalman G, Valtchinov V and Golden K I 1999 *Phys. Rev. Lett.* **82** 3124
[2] Golden K I and Kalman G 2000 *Phys. Plasmas* **7** 14
Golden K I and Kalman G 2001 *Phys. Plasmas* **8** 5064
[3] Donko Z, Kalman G J, Hartman P, Golden K I and Kutasi K 2003 *Phys. Rev. Lett.* **90** 226804
Donko Z, Hartman P, Kalman G J and Golden K I 2003 *J. Phys. A: Math. Gen.* **36** 5877
[4] Golden K I, Mahassen H, Kalman G J, Senatore G and Rapisarda F 2005 *Phys. Rev.* E **71** 036401
[5] Ranganathan S and Johnson R E 2004 *Phys. Rev.* B **69** 085310
[6] Vitlina R Z and Chaplik A V 1981 *Zh. Eksp. Teor. Fiz.* **81** 1011
Vitlina R Z and Chaplik A V 1981 *Sov. Phys.—JETP* **54** 536 (Engl. Transl.)
[7] Chaplik A V and Vitlina R Z 2003 *Superlatt. Microstruct.* **33** 263
[8] Kulik L V, Tovstonog S V, Kirpichev V E, Kukushkin I V, Dietsche W, Hauser M and Klitzing K V 2004 *Phys. Rev.* B **70** 033304
[9] Kalman G and Golden K I 1990 *Phys. Rev.* A **41** 5516
[10] Donko Z and Kalman G J 2001 *Phys. Rev.* E **63** 061504